

Microstructure and Mechanical Properties of As-Cast Al-Ti Based High Entropy Alloys with Ni-Cr-Sn and Ni-Fe-Sn Alloying Elements

Daniel Panghahatan Malau^{1,2*}, Albertus Deny Heri Setyawan², Deni Ferdian¹, and Yudi Nugraha Thaha²

¹Department of Metallurgy & Materials Engineering, Universitas Indonesia, Depok, Jawa Barat, Indonesia 16425

²Research Center for Metallurgy, National Research and Innovation Agency (BRIN), Kawasan Sains dan Teknologi B.J. Habibie, Tangerang Selatan, Banten, Indonesia 15314

Abstract. This study investigates the microstructure and mechanical properties of as-cast Al-Ti-Ni-based high entropy alloys (HEAs) alloyed with Cr-Sn and Fe-Sn. The alloys were produced by arc melting under an argon atmosphere without subsequent heat treatment. Microstructural analysis using optical metallography, scanning electron microscopy (SEM), and X-ray diffraction (XRD) revealed dendritic structures with interdendritic segregation. XRD results confirmed the presence of multiphase structures composed of body-centered cubic (BCC) solid solutions and intermetallic compounds. Mechanical behavior was evaluated through Vickers hardness and uniaxial compression testing, while theoretical densities calculated from alloy compositions were used to obtain specific hardness values ($HV \cdot cm^3/g$). Among the examined alloys, Al-Ti-Ni-Cr-Sn achieved a specific hardness of 90.21 and an ultimate compressive strength (UCS) of 1096 MPa, whereas Al-Ti-Ni-Fe-Sn recorded a specific hardness of 55.19 and a UCS of 515 MPa. Overall, the findings demonstrate that Al-Ti-Ni-based HEAs exhibit promising potential for lightweight, high-strength, and wear-resistant structural applications without the need for post-solidification processing.

1 Introduction

High-entropy alloys (HEAs) are a recently established class of materials, distinguished by their composition of five or more primary elements in near-equiatomic proportions [1,2]. Unlike conventional alloys, which are typically dominated by one or two main elements, the exceptional characteristics of HEAs stem from the complex and synergistic interactions among their multiple constituent elements. The equiatomic or near-equiatomic composition is instrumental in generating high configurational entropy, thereby stabilizing solid solution phases and preventing the formation of intermetallic compounds [3]. As a result, HEAs demonstrate a compelling range of properties, including impressive strength, excellent wear resistance, superior thermal stability, and notable corrosion resistance [4,5]. Among the many systems explored, aluminum-titanium (Al-Ti) based HEAs have gained interest due to their combination of low density, high specific strength, and good corrosion resistance, making them promising candidates for lightweight structural and high-temperature applications [2,6]. Alloying with Al typically promotes formation of ordered strengthening phases such as NiAl or γ' (Ni_3Al), while Ti contributes to solid solution strengthening and phase stability [7]. The incorporation of Ni, Cr and Sn into Al-Ti HEAs aims to enhance mechanical strength,

corrosion resistance, and phase stability. Ni and Cr can stabilize both FCC and BCC solid solution phases and promote oxidation resistance (Cr forming protective Cr_2O_3). Sn, although limited in solubility, may form fine precipitates that could refine microstructure or improve ductility [8]. An alternative design replaces Cr with Fe, producing AlTiNiFeSn compositions. Fe is less costly than Cr yet still promotes solid solution strengthening and refined microstructure due to its balanced mixing behaviour with Ni, Al, Ti, and Sn. Comparing AlTiNiCrSn and AlTiNiFeSn systems enables insight into how substituting Cr with Fe affects phase formation, elemental distribution, and microstructural refinement.

2 Materials and Methods

The AlTiNiFeCr alloy with equiatomic composition was synthesized using a high-purity arc melting process. High-purity elemental metals ($\geq 99.9\%$ purity) of aluminum, titanium, nickel, iron, and chromium were weighed and mixed in equiatomic ratios as shown in Tables 1 and 2. The mixture was melted in a water-cooled copper crucible under an inert argon atmosphere to prevent oxidation. The ingot was inverted between melting cycles and remelted five times to ensure chemical homogeneity, producing a 25 g button-shaped ingot measuring 25 mm in diameter and 5 mm in

* Corresponding author: dani005@brin.go.id

thickness, which was subsequently sectioned into test coupons with dimensions of 5 mm × 5 mm × 3 mm.

Table 1. Alloy composition for AlTiNiCrSn.

Element(s)	at. %	weight (g)
Al	20	2.217
Ti	20	3.936
Ni	20	4.823
Cr	20	4.272
Sn	20	9.752

Table 2. Alloy composition for AlTiNiFeSn.

Element(s)	at. %	weight (g)
Al	20	2.189
Ti	20	3.886
Ni	20	4.763
Fe	20	4.531
Sn	20	9.630

Optical metallography was performed to examine the macrostructure and grain structure of the alloy. Samples were prepared by standard metallographic techniques, including grinding, polishing, etching. Etching was done using a solution of 10% hydrofluoric acid (HF) and 90% distilled water. The etched samples were then observed under an optical microscope (Leica DM2700M) to capture images of the microstructure.

The phase identification of the alloy was conducted using X-ray diffraction (XRD). A PANalytical X'Pert PRO diffractometer with Cu K α radiation ($\lambda = 1.5406 \text{ \AA}$) was used. The diffraction patterns were collected over a 2θ range of 20° to 90° with a step size of 0.02° and a scanning rate of $1^\circ/\text{min}$. Phase identification was performed using the ICDD (The International Centre for Diffraction Data) database.

Microstructural analysis was carried out using a field emission scanning electron microscope (FE-SEM, JEOL JSM-7001F) equipped with an energy dispersive X-ray spectroscopy (EDS) system. Samples were mechanically polished and etched using a solution of 10% hydrofluoric acid (HF) and 90% distilled water to reveal the microstructure. The SEM images provided information on morphology, grain size, and elemental distribution of the alloy.

The specimen hardness was measured by a Vickers microhardness tester with an applied load of 0.49 N. A minimum of 10 tests were carried out on each specimen.

3 Results and Discussion

Fig. 1 shows the optical microstructures of AlTiNiCrSn and AlTiNiFeSn alloys, highlighting clear differences in their solidification behavior. The AlTiNiCrSn alloy (left) displays a coarse dendritic structure, which suggests that solidification occurred under non-equilibrium conditions, leading to element segregation, likely with Al and Sn concentrated in the interdendritic areas. This kind of structure indicates the

presence of multiple phases and uneven element distribution. On the other hand, the AlTiNiFeSn alloy (right) shows a much finer and more uniform microstructure, without clear dendritic patterns. This suggests that the replacement of Cr with Fe helps improve element mixing and reduces segregation. The addition of Fe appears to refine the microstructure, possibly by affecting how the solid phases form and grow.

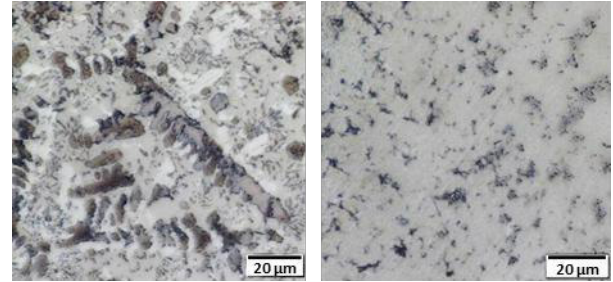


Fig. 1. Optical metallography of AlTiNiCrSn (left) and AlTiNiFeSn (right)

For AlTiNiCrSn alloys, the SEM microstructure (top left) and EDX elemental mapping are shown in Fig. 2 and 3, displaying the distribution of Al, Ti, Ni, Cr, and Sn. The SEM image reveals a dendritic microstructure, indicating that the alloy solidified under non-equilibrium conditions. The dendrites are well developed and show contrast differences, which suggest chemical segregation during solidification. The Al map (top right) shows a relatively uniform distribution with slightly higher concentration in the interdendritic regions. This is common in multi-component systems, where Al tends to segregate away from the primary dendrite cores. Chromium appears finely dispersed across the matrix. The uniform but slightly mottled distribution indicates minor segregation or the possible presence of fine Cr-rich phases. Nickel is present throughout the microstructure but shows some band-like variations, possibly due to segregation along the dendritic arms. These patterns align somewhat with the solidification features seen in the SEM image. Tin shows a relatively homogenous distribution, though some slight clustering may exist in certain regions. This may suggest Sn segregation or the formation of Sn-rich intermetallic phases, often observed in Al-based alloys with Sn. Titanium is dispersed across the matrix, with a relatively fine and uniform appearance. It does not show strong segregation, implying good solid solubility or very fine Ti-containing phases. The EDX mapping confirms that the AlTiNiCrSn alloy exhibits multi-elemental distribution with partial segregation during solidification. Al and Ni show a slight concentration variation in dendritic structures, while Ti and Cr are more uniformly distributed. Sn may form minor segregated regions or intermetallics.

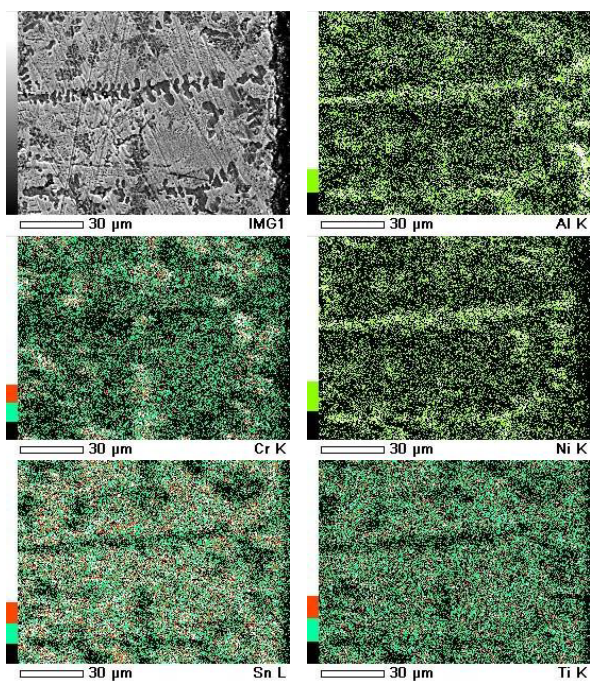


Fig. 2. SEM mapping of AlTiNiCrSn

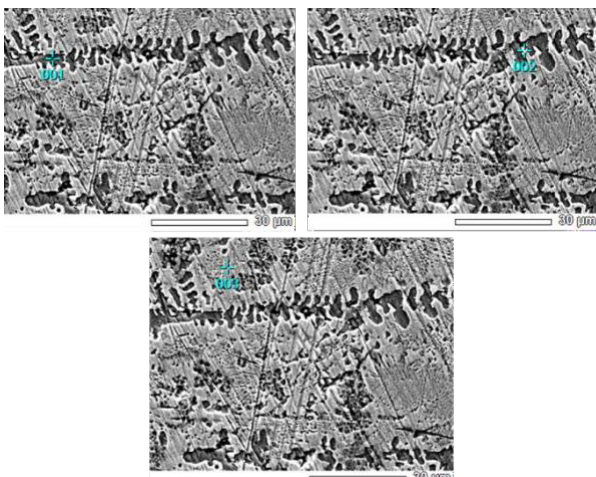


Fig. 3. SEM-EDS point analysis locations and corresponding elemental compositions for selected regions of the Al-Ni-Ti-Cr-Sn alloy.

The SEM image and EDX elemental maps of the AlTiNiFeSn alloy in Fig. 4 and 5 reveal a fine and relatively uniform microstructure. The SEM image reveals fine features without visible dendritic patterns, indicating improved solidification behavior. Elemental mapping confirms that Al, Fe, and Ti are evenly distributed throughout the matrix, suggesting good elemental mixing and minimal segregation. Nickel displays a slightly patterned distribution, possibly aligned with solidification directions, but remains fairly uniform overall. Tin shows some localized enrichment, indicating the possible formation of Sn-rich phases due to its limited solubility. The overall mapping results support that the substitution of Cr with Fe contributes to a more homogeneous elemental distribution and refined microstructure. This uniformity is expected to enhance the alloy's mechanical stability and corrosion resistance.

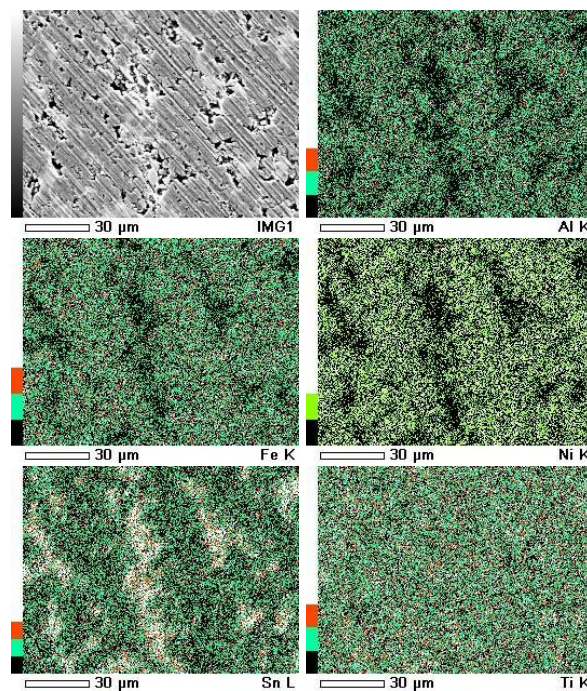


Fig. 4. SEM mapping of AlTiNiFeSn

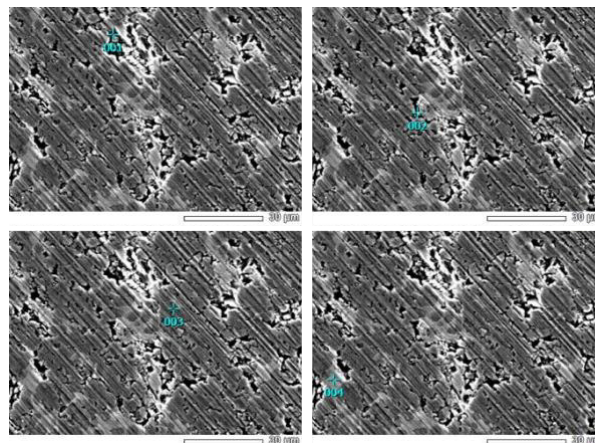


Fig. 5. SEM-EDS point analysis locations and corresponding elemental compositions for selected regions of the Al-Ni-Ti-Fe-Sn alloy.

Fig. 6 presents the XRD pattern of the Al-Ti-Ni-Cr-Sn alloy, revealing a multiphase structure characterized by the coexistence of Al-Ni-, Al-Ti-Ni-, Cr-Ti-Ni-, and Ni-Sn-based intermetallic phases. The dominant diffraction peaks correspond to the $Al_{0.88}Ni_{1.12}$ phase, indicating that the Al-Ni intermetallic constitutes the primary matrix. Additional reflections associated with $Al_{2.7}Ti_{1.07}Ni_{0.23}$ and $Cr_{1.75}Ni_{0.25}Ti$ phases confirm the incorporation of Ti and Cr into secondary intermetallic compounds. Moreover, the presence of $Ni_{1.38}Sn$ and $Ni_{0.78}Sn$ phases is evidenced by distinct low- to intermediate-angle peaks, suggesting Sn segregation and the formation of Ni-Sn intermetallics during solidification.

The phase assignments derived from XRD are strongly supported by EDS point analyses, which reveal pronounced local compositional heterogeneity (Table 3). At Test Point 1, the microstructure is dominated by an Al-rich and Ni-rich region (Al \approx 40.8 at.% and Ni \approx

53.6 at.%), consistent with a matrix primarily composed of $\text{Al}_{0.88}\text{Ni}_{1.12}$ (~92 – 93%), with minor contributions from $\text{Ni}_{1.38}\text{Sn}$ (~2 – 3%) and $\text{Cr}_{1.75}\text{Ni}_{0.25}\text{Ti}$ (~4 – 5%). Test Point 2 exhibits increased Ti and Sn contents, corresponding to a multiphase mixture consisting of $\text{Al}_{0.88}\text{Ni}_{1.12}$ (~51%), $\text{Al}_{2.7}\text{Ti}_{1.07}\text{Ni}_{0.23}$ (~21%), and $\text{Ni}_{1.38}\text{Sn}$ (~23%), indicative of interdendritic enrichment. In contrast, Test Point 3 shows substantial Ti, Cr, and Sn enrichment, and is best described by a combination of $\text{Al}_{2.7}\text{Ti}_{1.07}\text{Ni}_{0.23}$ (~20%), $\text{Cr}_{1.75}\text{Ni}_{0.25}\text{Ti}$ (~35%), and $\text{Ni}_{0.78}\text{Sn}$ (~44%), reflecting the formation of Sn-rich and Ti/Cr-rich secondary phases.

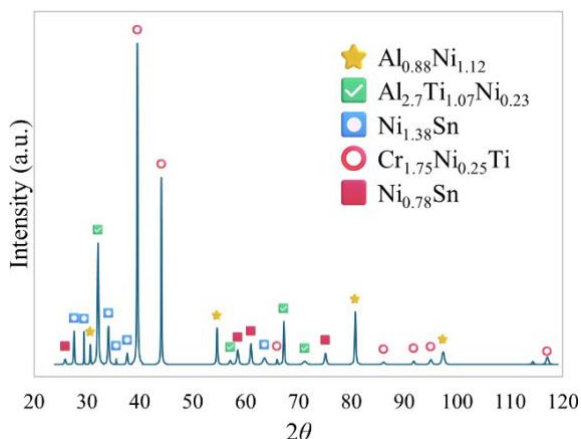


Fig. 6. XRD results of AlTiNiCrSn

Table 3. Elemental compositions (at.%) obtained from EDS point analyses at different test points and the corresponding possible phase constituents with estimated phase fractions in the Al-Ni-Ti-Cr-Sn alloy.

Test Point	Element Ratio (at. %)					Possible Phase(s) (approx. phase fraction, at.%)
	Al	Ti	Ni	Cr	Sn	
1	40.84	2.76	53.6	1.7	1.1	$\text{Al}_{0.88}\text{Ni}_{1.12}$ (~92–93%), $\text{Ni}_{1.38}\text{Sn}$ (~2–3%), $\text{Cr}_{1.75}\text{Ni}_{0.25}\text{Ti}$ (~4–5%)
2	35	9.31	44.46	3.27	7.96	$\text{Al}_{0.88}\text{Ni}_{1.12}$ (~51%), $\text{Al}_{2.7}\text{Ti}_{1.07}\text{Ni}_{0.23}$ (~21%), $\text{Ni}_{1.38}\text{Sn}$ (~23%)
3	7.04	34.98	13.56	11.75	32.68	$\text{Al}_{2.7}\text{Ti}_{1.07}\text{Ni}_{0.23}$ (~20%), $\text{Cr}_{1.75}\text{Ni}_{0.25}\text{Ti}$ (~35%), $\text{Ni}_{0.78}\text{Sn}$ (~44%)

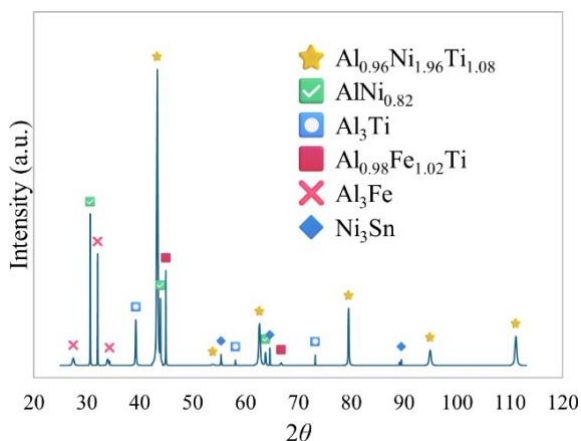


Fig. 7. XRD results of AlTiNiFeSn

Table 4. Elemental compositions (at.%) obtained from EDS point analyses at different test points and the corresponding possible phase constituents with estimated phase fractions in the Al-Ni-Ti-Fe-Sn alloy.

Test Point	Element Ratio (at. %)					Possible Phase(s) (approx. phase fraction, at.%)
	Al	Ti	Ni	Fe	Sn	
1	18.78	20.77	25.59	26.6	8.25	$\text{Al}_{0.96}\text{Ni}_{1.96}\text{Ti}_{1.08}$ (35%), $\text{Al}_{0.98}\text{Fe}_{1.02}\text{Ti}$ (30%), $\text{AlNi}_{0.82}$ (20%), Ni_3Sn (15%)
2	15.62	20.5	23.4	25.65	14.83	$\text{Al}_{0.96}\text{Ni}_{1.96}\text{Ti}_{1.08}$ (30%), $\text{Al}_{0.98}\text{Fe}_{1.02}\text{Ti}$ (30%), Ni_3Sn (25%), $\text{AlNi}_{0.82}$ (15%)
3	21.2	18.7	30.73	23.74	5.63	$\text{Al}_{0.96}\text{Ni}_{1.96}\text{Ti}_{1.08}$ (40%), $\text{Al}_{0.98}\text{Fe}_{1.02}\text{Ti}$ (30%), $\text{AlNi}_{0.82}$ (20%), Ni_3Sn (10%)
4	4.37	32.12	6.09	13.1	44.32	Ni_3Sn (55%), Al_3Ti (25%), $\text{Al}_{0.98}\text{Fe}_{1.02}\text{Ti}$ (20%)

Fig. 7 shows the X-ray diffraction (XRD) pattern of the Al-Ni-Ti-Fe-Sn alloy, indicating a complex multiphase structure. The diffraction peaks were indexed to several intermetallic phases, including $\text{Al}_{0.96}\text{Ni}_{1.96}\text{Ti}_{1.08}$, $\text{AlNi}_{0.82}$, Al_3Ti , $\text{Al}_{0.98}\text{Fe}_{1.02}\text{Ti}$, Al_3Fe , and Ni_3Sn . Among these, $\text{Al}_{0.96}\text{Ni}_{1.96}\text{Ti}_{1.08}$ is identified as the dominant phase, as evidenced by its high-intensity peaks across a wide 2θ range, suggesting that it forms the primary matrix of the alloy. The presence of $\text{AlNi}_{0.82}$ and $\text{Al}_{0.98}\text{Fe}_{1.02}\text{Ti}$ as secondary phases reflects the strong thermodynamic affinity of Al with Ni and Fe–Ti during solidification. Additional weak reflections corresponding to Al_3Ti and Al_3Fe indicate the existence of localized Al-rich regions. Furthermore, the clear detection of Ni_3Sn confirms that Sn preferentially reacts with Ni to form a stable intermetallic compound rather than remaining in solid solution within the Al-based matrix.

The compositional analysis obtained from EDS measurements at different test points (Table 4) is consistent with the XRD results and reveals notable chemical heterogeneity within the alloy. At test points 1 – 3, where Al, Ti, Ni, and Fe are present in relatively comparable proportions and the Sn content remains limited (approximately 5 – 15 at.%), the microstructure is dominated by $\text{Al}_{0.96}\text{Ni}_{1.96}\text{Ti}_{1.08}$ (30 – 40 at.%), accompanied by $\text{Al}_{0.98}\text{Fe}_{1.02}\text{Ti}$ (~30 at.%) and $\text{AlNi}_{0.82}$ (15 – 20 at.%). In these regions, the Ni_3Sn phase appears in smaller fractions (10 – 25 at.%), with its fraction increasing as the local Sn concentration rises. This trend indicates that Sn has a strong tendency to combine with Ni, promoting the formation of Ni_3Sn rather than participating in Al-Ti or Al-Fe intermetallic phases.

In contrast, test point 4 exhibits a distinctly different phase constitution, characterized by a significantly higher Sn content (44.32 at.%) and reduced Al and Ni concentrations. As a result, Ni_3Sn becomes the dominant phase (~55 at.%), while Al_3Ti (~25 at.%) and $\text{Al}_{0.98}\text{Fe}_{1.02}\text{Ti}$ (~20 at.%) are present as secondary phases. This observation confirms pronounced Sn microsegregation during solidification and highlights the limited solubility of Sn in the Al-Ti-Ni-Fe matrix.

The hardness of the AlTiNiCrSn and AlTiNiFeSn were compared with that of other HEAs and commercial alloys and is summarized in Table 5 [9 – 15]. Among

the listed alloys, AlTiNiCrSn exhibits a notably high specific hardness of 90.15 HV/(g/cm³), making it one of the top performers in terms of strength-to-weight ratio. Although its absolute hardness (540 HV) is slightly lower than that of AlCrMoTi (606 HV) and Al_{0.5}CoCrCuFeNiV (640 HV), the relatively low theoretical density of AlTiNiCrSn (5.99 g/cm³) contributes to its impressive specific hardness, which surpasses many conventional and high-entropy alloys. In contrast, AlTiNiFeSn displays a lower hardness of 336 HV and a specific hardness of 55.26 HV/(g/cm³), indicating that substituting Cr with Fe in the composition significantly reduces both hardness and strength-to-weight performance. Notably, AlTiNiCrSn outperforms several well-known materials such as Ti-6Al-4V and Inconel 718 in terms of specific hardness, suggesting its potential for lightweight structural applications where high mechanical performance is critical. These findings underscore the importance of alloying element selection in tailoring the mechanical properties of high-entropy alloys.

Table 5. Comparison of specific hardness of HEAs with other alloys.

Alloys	Hardness (HV)	Theoretical Density (g/cm ³)	Specific Hardness (HV/(g/cm ³))
AlTiNiCrSn	540 ± 34	5.99	90.15
AlTiNiFeSn	336 ± 37	6.08	55.26
AlCrMoTi [9]	606	6.01	100.83
AlCrMoTiV [9]	556	6.00	92.67
AlCoCrFeNi [10]	520	6.70	77.61
AlCoCrCuFeNi [11]	400	7.02	56.98
Al _{0.5} CoCrCuFeNiV [12]	640	7.27	88.03
Ti-6Al-4V [13]	346	4.43	78.10
Ti-6242 [14]	339	4.54	74.67
Inconel 718 [15]	355	8.18	43.40

4 Conclusion

In conclusion, this study has successfully characterized the microstructural and phase composition of AlTi-based high entropy alloys with alloying additions of Ni, Cr, Fe, and Sn using optical metallography, SEM/EDX, and XRD analyses. The results indicate that both the AlTiNiCrSn and AlTiNiFeSn systems exhibit multiphase structures composed of various intermetallic compounds, with the Cr-containing alloy demonstrating a coarser dendritic morphology and higher specific hardness compared to the Fe-containing variant. Conversely, the substitution of Cr with Fe yields a more refined and homogeneous microstructure, albeit with a reduction in hardness, suggesting a trade-off between structural uniformity and strength-to-weight performance. The observed

distribution of elements and identification of phases such as Al₃Ti, Al₃Fe, and Ni₃Sn underscore the complexity inherent in these alloys and the critical role of alloying elements in tailoring the overall properties. These findings not only enhance our understanding of phase formation and microstructural evolution in AlTi-based high entropy alloys but also provide valuable insights for future optimization aimed at balancing mechanical performance and lightweight design for advanced structural applications.

References

1. J.-W. Yeh, "Physical Metallurgy of High-Entropy Alloys," *JOM* **67**(10), 2254 – 2261 (2015).
2. D.B. Miracle, and O.N. Senkov, "A critical review of high entropy alloys and related concepts," *Acta Mater.* **122**, 448 – 511 (2017).
3. E.J. Pickering, and N.G. Jones, "High-entropy alloys: a critical assessment of their founding principles and future prospects," *Int. Mater. Rev.* **61**(3), 183 – 202 (2016).
4. P. Sathiyamoorthi, and H.S. Kim, "High-entropy alloys with heterogeneous microstructure: Processing and mechanical properties," *Prog. Mater. Sci.* **123**, 100709 (2022).
5. N. Hua, W. Wang, Q. Wang, Y. Ye, S. Lin, L. Zhang, Q. Guo, J. Brechtel, and P.K. Liaw, "Mechanical, corrosion, and wear properties of biomedical Ti-Zr-Nb-Ta-Mo high entropy alloys," *J. Alloys Compd.* **861**, 157997 (2021).
6. Y. Qiu, S. Thomas, M.A. Gibson, H.L. Fraser, and N. Birbilis, "Corrosion of high entropy alloys," *Npj Mater. Degrad.* **1**(1), 15 (2017).
7. H.-I. Jeong, J.-H. Kim, and C.-M. Lee, "Manufacturing of Ni-Co-Fe-Cr-Al-Ti High-Entropy Alloy Using Directed Energy Deposition and Evaluation of Its Microstructure, Tensile Strength, and Microhardness," *Materials (Basel)*. **17**(17), 4297 (2024).
8. A.M. Manzoni, S. Singh, H.M. Daoud, R. Popp, R. Völkl, U. Glatzel, and N. Wanderka, "On the path to optimizing the Al-Co-Cr-Cu-Fe-Ni-Ti high entropy alloy family for high temperature applications," *Entropy* **18**(4), (2016).
9. M. Kang, K.R. Lim, J.W. Won, K.S. Lee, and Y.S. Na, "Al-Ti-Containing Lightweight High-Entropy Alloys for Intermediate Temperature Applications," *Entropy* **20**(5), 355 (2018).
10. S.G. Ma, and Y. Zhang, "Effect of Nb addition on the microstructure and properties of AlCoCrFeNi high-entropy alloy," *Mater. Sci. Eng. A* **532**, 480–486 (2012).
11. C.-J. Tong, M.-R. Chen, S.-K. Chen, J.-W. Yeh,
12. T.-T. Shun, S.-J. Lin, and S.-Y. Chang, "Mechanical performance of the Al_xCoCrCuFeNi high-entropy alloy system

- with multiprincipal elements,” *Metall. Mater. Trans. A Phys. Metall. Mater. Sci.* **36**(5), 1263–1271 (2005).
13. M.-R. Chen, S.-J. Lin, J.-W. Yeh, S.-K. Chen, Y.-S. Huang, and M.-H. Chuang, “Effect of vanadium addition on the microstructure, hardness, and wear resistance of Al_{0.5}CoCrCuFeNi high-entropy alloy,” *Metall. Mater. Trans. A Phys. Metall. Mater. Sci.* **37**(5), 1363–1369 (2006).
 14. M. Niinomi, “Mechanical properties of biomedical titanium alloys,” *Mater. Sci. Eng. A* **243**(1–2), 231–236 (1998).
 15. W. Shen, A.B.O. Soboyejo, and W.O. Soboyejo, “Microstructural Effects on Fatigue and Dwell-Fatigue Crack Growth in α/β Ti-6Al-2Sn-4Zr-2Mo-0.1Si,” *Metall. Mater. Trans. A Phys. Metall. Mater. Sci.* **35 A**(1), 163–187 (2004).
 16. H.Z. Li, H. Zeng, and X.Q. Chen, “An experimental study of tool wear and cutting force variation in the end milling of Inconel 718 with coated carbide inserts,” *J. Mater. Process. Technol.* **180**(1–3), 296–304 (2006).